LOW-TEMPERATURE SOLID-STATE SYNTHESIS OF $FePO_4$ AS A HETEROGENEOUS FENTON-LIKE CATALYST FOR THE DEGRADATION OF METHYL BLUE **

Q. Zhang, X. Li, Q. Wang, S. Wang*

College of Chemistry and Materials Science, Fujian Normal University, Fuzhou, China; e-mail: *wangsm@fjnu.edu.cn*

A potential iron phosphate ($FePO_4$) catalyst was prepared using a low-temperature solid-state method for the heterogeneous Fenton-like degradation of methyl blue (MB). A variety of parameters affecting the MB removal rate, including temperature, initial pH, catalyst usage, H_2O_2 and MB concentration, was studied in detail. The prepared $FePO_4$ exhibited a highly efficient catalytic reaction with seven cycle performance. In addition, a free radical masking experiment revealed the existence of a hydroxyl radical (•OH) and indicated that the degradation of MB was mainly due to the oxidation caused by •OH. This work suggests $FePO_4$ is an efficient material, which is responsible for the catalytic degradation of the azo dye MB through a heterogeneous Fenton-like system.

Keywords: *heterogeneous Fenton-like, ferric phosphate, hydroxyl radical, low-temperature solid-state reaction.*

НИЗКОТЕМПЕРАТУРНЫЙ ТВЕРДОТЕЛЬНЫЙ СИНТЕЗ $FePO_4$ КАК ГЕТЕРОГЕННОГО ФЕНТОНОПОДОБНОГО КАТАЛИЗАТОРА РАЗЛОЖЕНИЯ МЕТИЛЕНОВОГО СИНЕГО

Q. Zhang, X. Li, Q. Wang, S. Wang*

УДК 546.07:66.097.3

Колледж химии и материаловедения Фуцзяньского педагогического университета, Фучжоу, Китай; e-mail: *wangsm@fjnu.edu.cn*

(Поступила 11 февраля 2020)

Потенциальный катализатор на основе фосфата железа ($FePO_4$) для гетерогенного фентоноподобного разложения метиленового синего (МС) получен методом низкотемпературного твердотельного синтеза. Изучены параметры, влияющие на скорость разложения МС: температура, начальный pH, наличие катализатора, концентрации H_2O_2 и МС. Приготовленный $FePO_4$ показал высокоэффективную каталитическую реакцию за семь циклов. Эксперимент по маскировке свободных радикалов выявил существование гидроксильного радикала (•OH) и показал, что разложение МС происходит в основном из-за окисления, вызванного •OH. Предполагается, что $FePO_4$ эффективен как каталитизатор разложения азокрасителя МС через фентоноподобную гетерогенную систему.

Ключевые слова: *гетерогенное фентоноподобное разложение, фосфат железа, гидроксильный радикал, низкотемпературная твердотельная реакция.*

Introduction. Printing and dyeing wastewater contributes a lot to water pollution [1]. The non-biodegradable organic matter abundant in it shows a dark color and high chemical oxygen demand and other peculiarities [2]. Currently, photocatalytic [3], electro-Fenton [4], and Fenton-like processes are widely applied for its treatment [5–7]. The Fenton process presents significant advantages in the catalytic oxidation of high-concentration and non-biodegradable organic dyes. Since the traditional homogeneous Fenton process has some limitations such as difficulty to store and transport hydrogen peroxide (H_2O_2), the heterogeneous Fenton-like process has received considerable attention for its better catalytic oxidation, ease of reuse, and absence of secondary pollution [8–10].

**Full text is published in JAS V. 89, No. 1 (http://springer.com/journal/10812) and in electronic version of ZhPS V. 89, No. 1 (http://www.elibrary.ru/title_about.asp?id=7318; sales@elibrary.ru).

Ideally, the development of a Fenton-like environment friendly, high effective catalyst with low energy consumption is the key to the environmental organic pollution control technology. Most of the metal phosphates have a robust skeleton structure and excellent stability, which shows an extensive application prospect in the field of catalysis and adsorption. As a member of the metal phosphate group, $FePO_4$ is widely used in the field of catalytic wastewater purification [11–13]. Zhou et al. prepared graphene oxide-$FePO_4$ nanocomposites that can act as Fenton-like catalysts and display improved catalytic activities in the degradation of methyl blue (MB) [14]. In addition, the low-temperature solid-state reaction belongs to "green chemistry" because its strength lies in simple operation, absence of solvent, less pollution, and high yield [15–17].

Herein, combining the environmental friendliness characteristics of the low-temperature solid-phase method and the favorable physicochemical properties of the $FePO_4$ catalyst, in our work the $FePO_4$ sample was prepared by the low-temperature solid-phase method as a heterogeneous Fenton catalyst. Meanwhile, various factors influencing the degradation of MB were studied in detail, covering the catalytic reaction mechanism and cyclicity of MB.

Experimental methods. $FePO_4$ was synthesized by the low-temperature solid-state reaction. In brief, ferric chloride ($FeCl_3 \cdot 6H_2O$, AR) and sodium phosphate ($Na_3PO_4 \cdot 12H_2O$, AR) were mixed at a molar ratio 1:1 and then ground at room temperature for 40–60 min. The color of the mixture gradually became shallow, and then (after the reaction) the mixture appeared as a pale-yellow solid. After that we washed the sample several times with deionized water and dried it at 90°C for 6 h to obtain a linen-colored powder.

The crystal structure of $FePO_4$ was characterized by X-ray diffraction (XRD, PHLIPS X' Pert MPD); CuK_α (40 kV, 40 mA, $\lambda = 0.1541$ nm) was the radiation source, with scan rate 2°/min, $2\theta = 10–80°$. The surface microscopic structure was observed by field-emission scanning electron microscopy (FESEM, S4800, Hitachi, Japan); the elemental composition and content were detected by energy disperse spectroscopy (EDS, S4800, Hitachi, Japan). We used X-Ray photoelectron spectroscopy to analyze the elemental composition and chemical valence of each element (XPS, Kratos AXIS Ultra DLD, KRATOS, Japan), and Fourier-transform infrared spectroscopy to analyze the function group (FT-IR, NEXUS 670, Nicolet, USA) by the KBr tablet method. The scanning range was 4000–400 cm^{-1}.

The catalytic activity of $FePO_4$ was evaluated by MB degradation. An amount of the MB solution was added to the Erlenmeyer flask. After adding the catalyst, the pH of the solution was adjusted with the H_2SO_4 or NaOH solution. The solution was stirred for 20 min to reach the adsorption-separation equilibrium. The data point was collected from the absorbance of the 4 mL centrifuged supernatant at 664 nm with a UV-vis spectrophotometer. The sample concentration was expressed in C_0. Then, a certain concentration of H_2O_2 (30%, AR) was added to the solution for reaction. The samples were measured every 10 min in the same way as before. The sample concentration was expressed by C_n and the decolorization rate: $D = (C_0 - C_n)/C_0 \times 100\%$.

Results and discussion. The XRD patterns of $FePO_4$ are shown in Fig. 1a. Compared to the amorphous form before calcination, the diffraction peaks of the sample after calcination correspond to the $FePO_4$ crystal planes (JCPDS #50-1635). The impurity phase is not seen in the pattern, indicating that $FePO_4$ is successfully synthesized through a low-temperature solid-phase reaction. The FT-IR spectra of $FePO_4$ and Na_3PO_4 are shown in Fig. 1b. KBr is chosen as a diluent. The strong absorption peaks at 3650–3100 and 1600 cm^{-1} belong to the stretching and bending vibration of -OH [18]. The absorption peaks at 1050 and 540 cm^{-1} assigned to PO_4^{3-} [19]. They show that both $FePO_4$ and Na_3PO_4 have strong absorption to PO_4^{3-} and -OH. The absorption peaks of Na_3PO_4 at 1013 and 542 cm^{-1} correspond to the stretching and bending vibration of P-O. The peaks of $FePO_4$ at 1042 and 550 cm^{-1} attributed to the stretching vibration of P-O and Fe-O, respectively. The bending vibration of P-O is not obvious due to the overlap of Fe-O and tensile vibration. The absorption peak at 738 cm^{-1} belongs to the tensile vibration of Na-O that exists in Na_3PO_4 rather than $FePO_4$. It shows that Na_3PO_4 is thoroughly converted to form the structure of $FePO_4$.

XPS characterization of the heat-treated $FePO_4$ is tested to analyze the elemental composition and valence of $FePO_4$. The presence of elemental Fe, P, and O in the prepared sample was confirmed by the full spectrum in Fig. 2a. The spectrum of Fe 2*p* is shown in Fig. 2b; the peaks located at 724.7 and 713.9 eV are attributed to Fe $2p_{1/2}$ and Fe $2p_{3/2}$, respectively. The differences of Fe in Fe_2O_3 and $FePO_4$ lead to inconsistent binding energy [20, 21]. The corresponding binding energy of the P spectrum (Fig. 2c) is at 132.9 eV, indicating that the valence of P in the samples is +5 [22]. There are different kinds of O chemical bonds of $FePO_4$, including P-O, Fe-O, H-O (Fig. 2d). The characteristic peaks at 532.6 eV correspond to P-O and Fe-O, and the peak at 531.2 eV corresponds to -OH [23, 14].

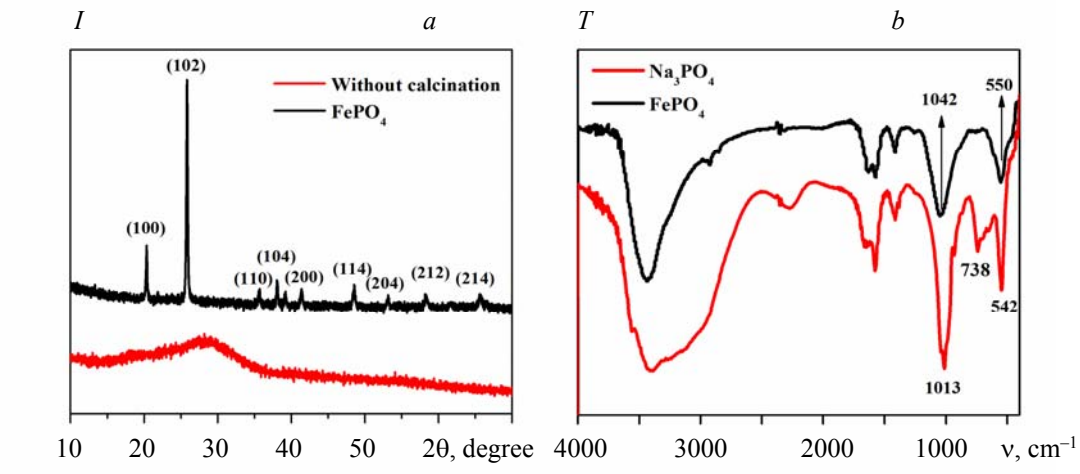

Fig. 1. a) XRD; b) FTIR patterns of samples.

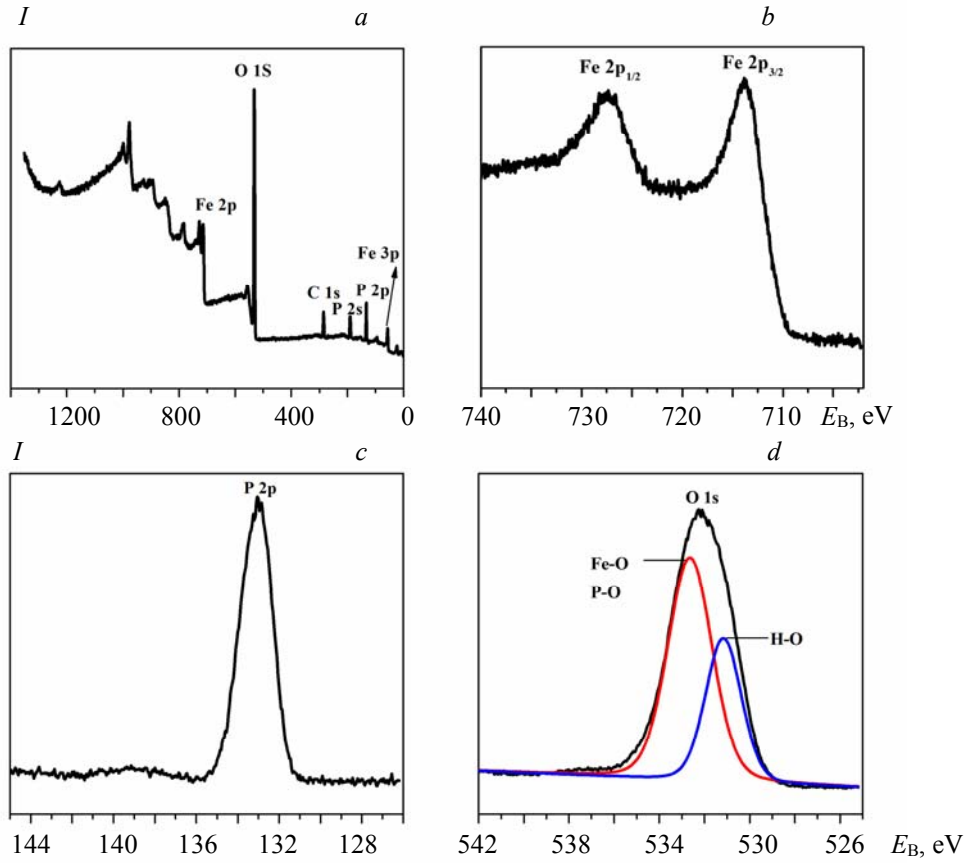

Fig. 2. XPS spectrum of $FePO_4$.

In order to determine the morphology of the $FePO_4$ microscopic surface, SEM characterization was carried out. Figure 3a reveals the loose layer structure of the $FePO_4$ sample, where most agglomerated particles are bigger than 2 μm. Generally, the structure may provide a large specific surface area. EDS is used to determine the elemental composition and content on the surface of the $FePO_4$ sample (Fig. 3b). The EDS results confirm the presence of elemental Fe, O, P in the sample and the approximate atomic ratio of 1:1 for elemental Fe and P, which is in line with the stoichiometric ratio of $FePO_4$ [24]. This demonstrates the successful formation of the Fe-P alloy in the $FePO_4$ catalyst.

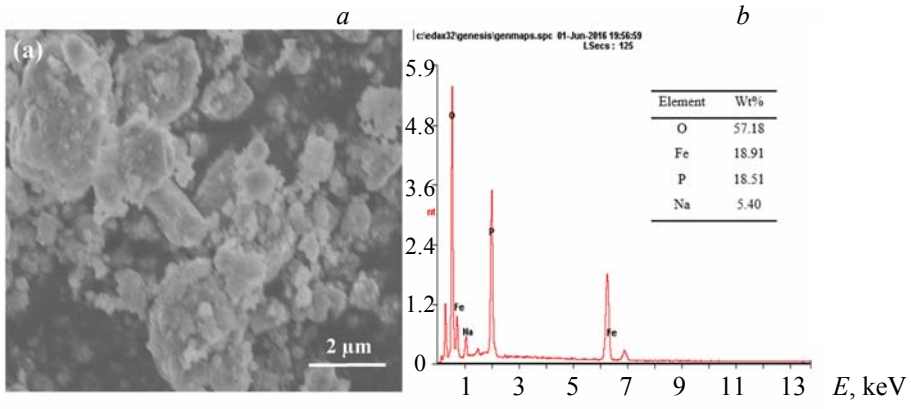

Fig. 3. a) SEM; b) EDS images of the samples.

The experimentations on the $FePO_4$ catalytic degradation of MB under various conditions were performed (Scheme 1). Under the experimental conditions (pH 3.0, T = 50°C, 5 mmol/L H_2O_2, 0.50 g/L catalyst, 100 mg/L MB), the influence of each factor was investigated by the controlled variable method.

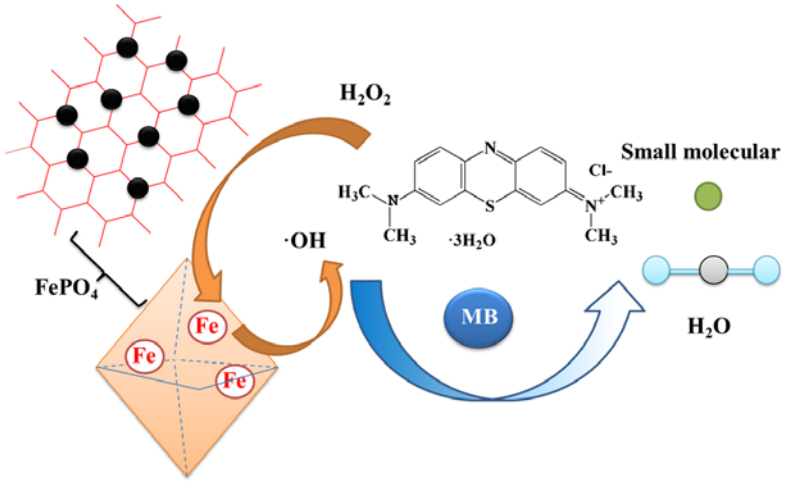

Scheme 1. Schematic presentation of $FePO_4$ sample degrading MB.

The comparison results of the three systems ($FePO_4$, H_2O_2, $FePO_4$ + H_2O_2) are presented in Fig. 4a. The degradation rate of the MB solution reaches 99% within 20 min in the $FePO_4$ + H_2O_2 system, while the degradation rates in the $FePO_4$ or H_2O_2 system are just 6 and 18% after 60 min of reaction. This proves that $FePO_4$ has efficient catalytic activity for the H_2O_2 oxidation degraded MB solution. pH is one of the significant parameters in the Fenton-like process, since pH greatly affects the production of •OH [18]. Figure 4b exhibits the experimental results for different initial pH conditions. The results show that the optimal pH value is 3.0. The results comply with the law of the Fenton process, which means that the concentration of •OH is higher under acidic conditions. Actually, high-valence iron ions (Fe^{4+}) have replaced •OH in alkaline conditions, and the oxidation of Fe^{4+} is weaker than •OH [25]. It shows that the degradation rate of MB decreases with increasing pH value. To observe the effect of temperature on the degradation performance, experiments were carried out at 28, 40, and 50°C. As shown in Fig. 4c, the degradation rate of MB reaches 99% within 30 min when the reaction temperature rises to 50°C. The generation rate of •OH and the degradation rate of organic pollutants can be significantly improved at an appropriate high temperature. More notably, the rate of the H_2O_2 solution decomposed into oxygen increases with temperature, so excessive temperature is not conducive to the degradation of organic pollutants [26]. Further investigations were implemented to clarify the effects of the H_2O_2 concentration on the Fenton-like degradation. Figure 4d clearly shows that the degradation rate of MB is promoted with increase in H_2O_2 concentration (within 5 mmol/L). The hydroxyl radical only derives from H_2O_2 in the experiment, so the concentration of H_2O_2 should be pro-

portional to the degradation rate [21]. When the concentration [H_2O_2] > 5 mmol/L, the degradation rate hardly continues to rise. In contrast, the degradation rate of MB shows a downward trend when the H_2O_2 concentration reaches 20 mmol/L. This can be ascribed to the scavenging of •OH radicals by the excess presence of H_2O_2, resulting in a decrease in the •OH content in the system [23]. Furthermore, the effect of the catalyst dosage is illustrated in Fig. 4e. It seems that the dosages of the catalyst within 0.50 g/L are fairly stable for the degradation operation. However, the degradation rate of MB increased by 1.00 g/L, which means that the overfull active sites on the catalyst surface can remove •OH partly. Moreover, the excessive catalyst reduces the density of •OH on the catalyst surface, which ultimately leads to a decrease in the degradation rate [26, 27]. Based on the above experimental results, the degradation of different concentrations of MB was further investigated. As presented in Fig. 4f, the initial MB concentrations were 150 and 200 mg/L, and the degradation rates reach 82 and 71%, respectively. Although increasing the concentration of MB slowed down the degradation rate, the total amount of degradation increases. As the concentration of pollutants increases, many organic pollutants are prone to occupy active sites on the catalyst surface. Hydrogen peroxide cannot contact the active site, and the system only generates insufficient •OH, thereby leading to a reduction in the MB degradation rate [28].

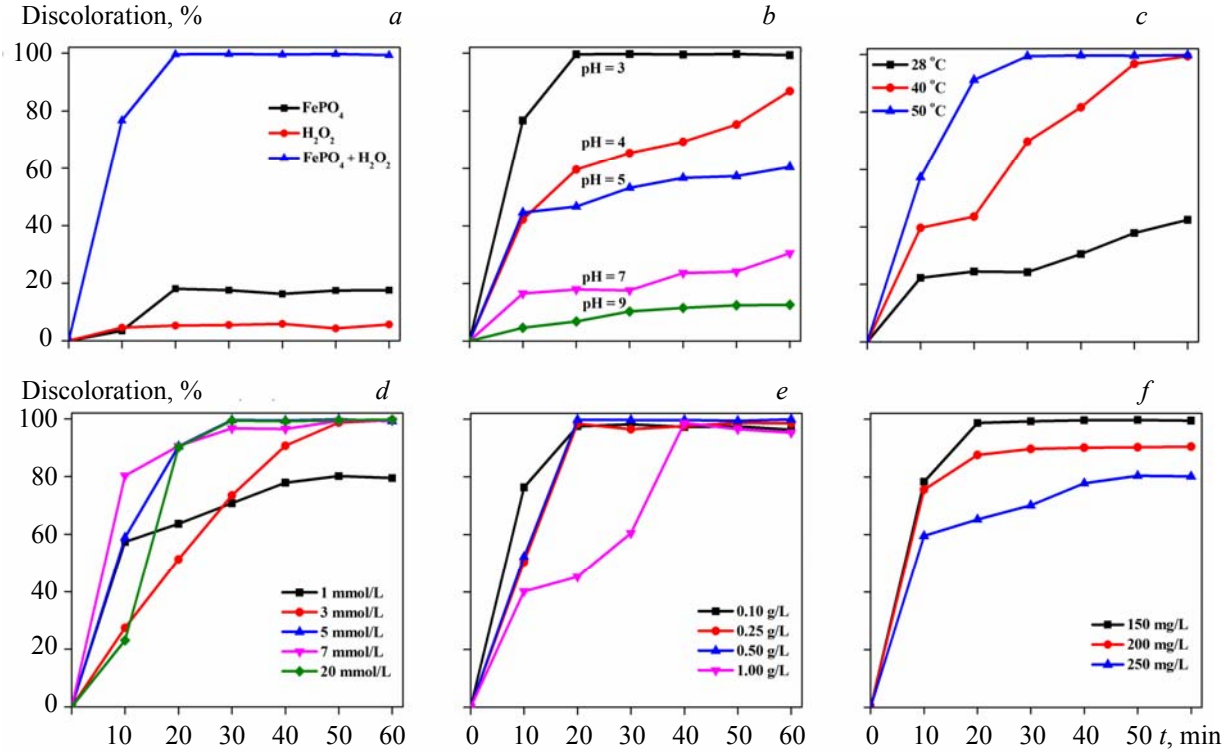

Fig. 4. Effect of the different (a) systems, (b) initial pH values, (c) temperatures, (d) H_2O_2 concentrations, (e) catalyst dosages, and (f) MB concentrations on the degradation of MB.

Traditionally, the Fenton-like reaction mechanism is the mechanism of hydroxyl radicals that removes organic pollutants in wastewater owing to the strong oxidation function of •OH. To identify the hydroxyl radicals as a major active oxygen species involved in the $FePO_4 + H_2O_2$ system, isopropanol (C_3H_8O) was chosen as the radical quencher due to its high reactivity toward •OH. We compared the two systems $FePO_4 + H_2O_2$ and $FePO_4 + H_2O_2 + C_3H_8O$ under the same experimental conditions. Obviously, the MB degradation rate is sharply reduced in systems containing isopropanol, as evident from Fig. 5a. It shows a large amount of •OH radicals generated in the $FePO_4 + H_2O_2$ system and proves that the degradation of organic pollutants in this experiment complies with the hydroxyl radical mechanism of the Fenton-like reaction. The •OH radical has the ability to degrade organic pollutants due to its strong oxidation and accelerated generation in the acidic environment. As seen in Fig. 5b, $FePO_4$ can indeed effectively degrade MO, X-3B, and K-nr under the same experimental conditions. The results further verify that the degradation of organic pollutants in this experiment is based on the hydroxyl radical mechanism. The UV-Vis spectrum is displayed in Fig. 5c. The

characteristic peaks of 664, 245, and 293 nm decrease rapidly with the extension of the reaction time. It shows that the large molecules in the MB solution are broken down into small molecules, leaving benzene or other small molecules. The results demonstrate that $FePO_4$ catalyzes the generation of •OH from hydrogen peroxide to promote the decomposition of MB. According to Fig. 5d, the stability and recyclability of $FePO_4$ catalysts were evaluated under optimal conditions. The MB degradation declined in the 7th cycle. However, a removal efficiency of 96.8% is still maintained. This may be attributed to the adsorption of intermediates and the coverage of active surface sites by organics.

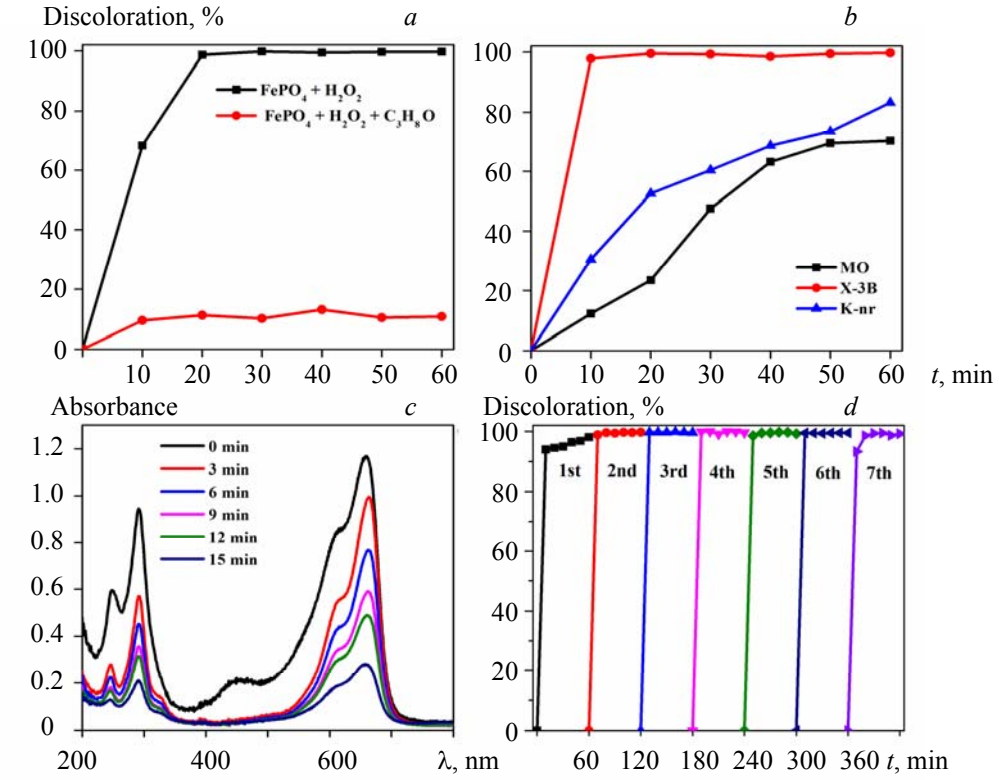

Fig. 5. a) Effect of isopropanol on the discoloration of X-3B; b) degradation curves of different dyes; c) UV-Vis spectra at different reaction times; d) the recycling of $FePO_4$; pH 3.0, 50°C, 5 mmol/L H_2O_2, 0.50 g/L catalyst, 100 mg/L MB.

Conclusions. A green energy-saving route of low-temperature solid-state reaction to synthesize the $FePO_4$ catalyst is proposed. The kinetic studies indicate that $FePO_4$ effectively degrades organic wastewater simulated by the MB dye with the appropriate catalyst dosage, H_2O_2 concentration, reaction temperature, and pH value. In addition, •OH is believed to be the primary radical in the Fenton-like process. The efficiency of the catalyst cycle degradation remains stable. Comprehensively, $FePO_4$ is a highly efficient heterogeneous Fenton-like catalyst with broad prospects in the field of wastewater treatment.

Acknowledgments. This work was supported by the National Engineering Research Center of Chemical Fertilizer Catalyst (NERC-CFC), Fuzhou University.

REFERENCES

1. G. Zhang, I. Okajima, T. Sako, J. Supercrit, *Fluids*, **112**, 136–142 (2016).
2. M. Chethana, L. G. Sorokhaibam, V. M. Bhandari, S. Raja, V. V. Ranade, *ACS Sustain. Chem. Eng*., **4**, No. 5, 2495–2507 (2016).
3. Z. Han, N. Wang, H. Zhang, X. Yang, *J. Appl. Spectrosc.*, **83**, No. 6, 1007–1011 (2017).
4. Y. H. Zhang, B. Lai, Y. X. Zhou, J. L. Wang, P. Yang, *J. Appl. Spectrosc*., **80**, No. 5, 681–693 (2013).
5. K. Plakas, A. Mantza, S. Sklari, V. Zaspalis, A. Karabelas, *Chem. Eng. J.*, **373**, 700–708 (2019).

6. D. Huang, C. Hu, G. Zeng, M. Cheng, P. Xu, X. Gong, R. Wang, W. Xue, *Sci. Tot. Environ.*, **574**, 1599–1610 (2017).
7. Y. Wang, C. Feng, Y. Li, J. Gao, C.-P. Yu, *Chem. Eng. J.*, **307**, 679–686 (2017).
8. S. Tao, J. Yang, H. Hou, S. Liang, K. Xiao, J. Qiu, J. Hu, B. Liu, W. Yu, H. Deng, *Chem. Eng. J.*, **372**, 966–977 (2019).
9. M. Cheng, C. Lai, Y. Liu, G. Zeng, D. Huang, C. Zhang, L. Qin, L. Hu, C. Zhou, W. Xiong, *Coord. Chem. Rev.*, **368**, 80–92 (2018).
10. R. Zhou, X. Zhang, K. Bazaka, K. K. Ostrikov, *Front. Chem. Sci. Eng.*, **13**, No. 2, 340–349 (2019).
11. C. Nadejde, M. Neamtu, V. D. Hodoroaba, R. J. Schneider, A. Paul, G. Ababei, U. Panne, *J. Nanopart. Res.*, **17**, No. 12, 476 (2015).
12. D. Li, C. Pan, R. Shi, Y. Zhu, *Cryst. Eng. Commun.*, **13**, 6688–6693 (2011).
13. Z. J. Li, G. Ali, H. J. Kim, S. H. Yoo, S. O. Cho, *Nanoscale Res. Lett.*, **9**, No. 1, 276 (2014).
14. H. Zhou, X. Yue, H. Lv, L. Kong, Z. Ji, X. Shen, *Ceram. Int.*, **44**, 7240–7244 (2018).
15. W. Chen, Y. Chen, W. Wu, T. Li, C. Zhang, Y. Zhou, J. Wu, *J. Supercond. Nov. Magn.*, **29**, No. 1, 115–122 (2016).
16. H. Xu, V. Vuorinen, H. Dong, M. Paulasto-Kröckel, *J. Alloy. Compd.*, **619**, 325–331 (2015).
17. P. Hao, Z. Zhao, J. Tian, Y. Sang, G. Yu, H. Liu, S. Chen, W. Zhou, *Acta Mater.*, **62**, 258–266 (2014).
18. N. Inchaurrondo, J. Font, C. P. Ramos, P. Haure, *Appl. Catal. B-Environ.*, **181**, 481–494 (2016).
19. M. Khachani, A. El Hamidi, M. Kacimi, M. Halim, S. Arsalane, *Thermochim. Acta*, **610**, 29–36 (2015).
20. S. Y. Lee, D.-H. Kim, S. C. Choi, D.-J. Lee, J. Y. Choi, H.-D. Kim, *Microporous Mesoporous Mater.*, **194**, 46–51 (2014).
21. G. Yang, B. Ding, J. Wang, P. Nie, H. Dou, X. Zhang, *Nanoscale*, **8**, No. 16, 8495–8499 (2016).
22. Y. Yin, H. Zhang, P. Wu, B. Zhou, C. Cai, *Nanotechnology*, **21**, No. 42, 425504 (2010).
23. X. Wang, W. Yang, Y. Ji, X. Yin, Y. Liu, X. Liu, F. Zhang, B. Chen, N. Yang, *RSC Adv.*, **6**, 26155–26162 (2016).
24. X. Guan, J. Chang, Z. Xu, Y. Chen, H. Fan, *RSC Adv.*, **6**, No. 35, 29054–29063 (2016).
25. L. Qin, G. Zhang, Z. Fan, Y. Wu, X. Guo, M. Liu, *Chem. Eng. J.*, **244**, 296–306 (2014).
26. N. Wang, T. Zheng, G. Zhang, P. Wang, *J. Environ. Chem. Eng.*, **4**, No. 1, 762–787 (2016).
27. A. Cihanoğlu, G. Gündüz, M. Dükkancı, *Appl. Catal. B Environ.*, **165**, 687–699 (2015).
28. S. Wang, C. Zhao, D. Wang, Y. Wang, F. Liu, *RSC Adv.*, **6**, No. 23, 18800–18808 (2016).